

High-Performance and Long-Lived Cu/SiO₂ Nanocatalyst for CO₂ Hydrogenation

Zhi-Qiao Wang,^{†,‡} Zhong-Ning Xu,^{*,†,‡} Si-Yan Peng,[†] Ming-Jian Zhang,[†] Gang Lu,[†] Qing-Song Chen,[†] Yumin Chen,[†] and Guo-Cong Guo^{*,‡}

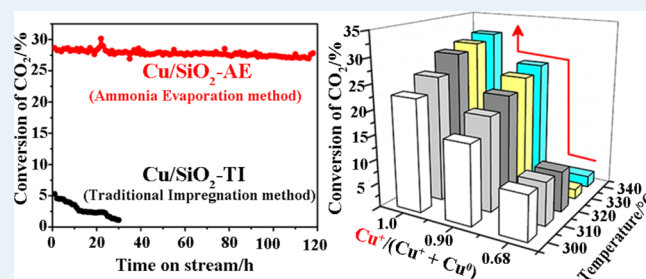
[†]State Key Laboratory of Structural Chemistry, Fujian Institute of Research on the Structure of Matter, Chinese Academy of Sciences, Fuzhou, Fujian 350002, People's Republic of China

[‡]Key Laboratory of Coal to Ethylene Glycol and Its Related Technology, Chinese Academy of Sciences, Fuzhou, Fujian 350002, People's Republic of China

S Supporting Information

ABSTRACT: Cu-based nanocatalysts have been widely used for CO₂ hydrogenation, but their poor stability is the bottleneck for further industrial applications. A high-performance and long-lived Cu/SiO₂ nanocatalyst was synthesized by an ammonia-evaporation method for CO₂ hydrogenation. The conversion of CO₂ reaches up to 28%, which is close to the equilibrium conversion of CO₂ (30%), and the selectivity to methanol is 21.3%, which is much higher than the equilibrium selectivity (6.6%) at 320 °C and 3.0 MPa. Furthermore, after 120 h of evaluation, the conversion can be still maintained at a high value (27%), which is much better than a Cu/SiO₂ catalyst prepared by traditional impregnation. The Cu⁺ species has been demonstrated to be the active component for the activation and conversion of CO₂. The higher ratio of Cu⁺/(Cu⁰ + Cu⁺) and interaction between the metal and support deriving from copper phyllosilicate are mainly responsible for the high catalytic activity and excellent stability, respectively.

KEYWORDS: ammonia-evaporation method, Cu/SiO₂ nanocatalyst, CO₂ hydrogenation, copper phyllosilicate, Cu⁺ species



One of the main “greenhouse gases” is CO₂, which is produced by the utilization of carbon-rich fossil fuels (e.g., coal, oil, and natural gas).^{1,2} In recent decades, the rapidly raising concentration of CO₂ in the atmosphere has resulted in a series of environment problems, such as global warming, ocean acidification, climate change, and so on.^{3–5} Although natural photosynthesis can convert CO₂ to organic carbon, it is far from enough to consume so much CO₂ in a short period with its increasing concentration.⁶ Recently, the catalytic conversion of CO₂ has attracted much attention because it can not only close the anthropogenic carbon cycle but also provide useful chemicals, such as epoxides, methanol, formic acid, and so on.^{7–13} However, few industrial processes have utilized CO₂ as a raw material to produce high-value chemicals.¹⁴ The biggest challenge is that CO₂ activating requires a large amount of energy because of a lack of effective catalysts.^{15,16} Hence, it is quite essential to develop high-performance catalysts to activate and convert CO₂ under mild conditions.^{17,18}

Cu-based nanocatalysts have been widely used in the field of CO₂ hydrogenation because of their high activity for activation and conversion of CO₂.^{19–27} The catalytic activity of Cu-based nanocatalyst would dramatically improve with a decrease in the Cu particle size;²⁸ however, Cu-based nanocatalysts are not stable because Cu nanoparticles (NPs) would easily aggregate and sinter during the preparation and use processes.²⁹ Notably,

the growth of metal NPs, which can result in loss of active surface area, is the main reason for deactivation of many supported nanocatalysts.²⁹ The poor stability of Cu NPs is the bottleneck for industrial application.^{30,31} Introducing structure promoters has been used to mitigate the growth of Cu NPs,^{32,33} but sometimes it just does not work because it would restrict the chemical composition and functionality of Cu-based nanocatalysts.^{29,34,35} Hence, developing a new strategy to prepare high-performance and long-lived supported Cu-based nanocatalysts without any promoter has important significance for activation and conversion of CO₂.

In this work, a high-performance and long-lived Cu/SiO₂ nanocatalyst (denoted as Cu/SiO₂-AE; see the preparation process details in the Supporting Information (SI)) has been synthesized by an ammonia-evaporation (AE) method.³⁶ CO₂ hydrogenation to methanol was chosen as a probe reaction to evaluate the Cu/SiO₂-AE nanocatalyst.

Figure 1 presents the performances of the Cu/SiO₂-AE nanocatalyst for the hydrogenation of CO₂ to methanol. The products of the Cu/SiO₂-AE nanocatalyst for CO₂ hydrogenation are methanol, CO, and a small amount of methane.

Received: August 10, 2014

Revised: May 25, 2015

Published: June 8, 2015

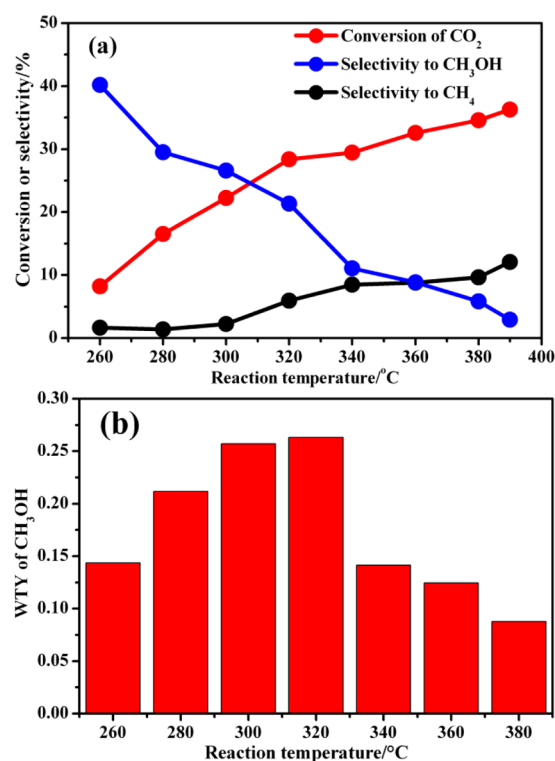


Figure 1. Performances of the Cu/SiO₂-AE nanocatalyst for CO₂ hydrogenation^[i]: (a) Conversion of CO₂, selectivity to CH₃OH and selectivity to CH₄ as functions of reaction temperature, (b) WTY^[ii] of methanol as functions of reaction temperature. ^[i] Reaction conditions: 0.3 g catalyst, 3.0 MPa, weight hour space velocity (WHSV) = 16 L·g_{cat}⁻¹·h⁻¹, H₂: CO₂ = 4:1. ^[ii] WTY represents the weight-time yield, grams of methanol per gram of catalyst per hour (g_{cat}⁻¹·h⁻¹).

With the increase of the reaction temperature from 260 to 380 °C, the conversion of CO₂ increases from 8.2 to 35.0%, and the selectivity to methanol decreases from 40.2% to 5.9%, implying that a low temperature is suitable for the synthesis of methanol but not for CO₂ catalytic conversion³⁷ (Figure 1a). The conversion of CO₂ at 320 °C is close to the equilibrium conversion (30%, Table S1), suggesting the as-synthesized Cu/SiO₂-AE nanocatalyst is of high activity for CO₂ hydrogenation. Interestingly, the selectivity to methanol at 320 °C is 21.3%, which is much higher than that (6.6%, Table S1) of the equilibrium selectivity to methanol (Figure S1). The main product, CO, can further hydrogenate to methanol over the Cu/SiO₂-AE nanocatalyst (Figure S2). The influence of WHSV has been presented in Figure S3. The weight time yield (WTY) of methanol presents the volcanic type trend and reaches the maximum of 0.26 g_{cat}⁻¹·h⁻¹ at 320 °C, according to the conversion and selectivity (Figure 1b). Most importantly, the conversion of CO₂ over the Cu/SiO₂-AE nanocatalyst can still maintain at a high value (27%) after 120 h of evaluation (Figure 2), which indicates that the as-synthesized Cu/SiO₂-AE nanocatalyst is quite stable and has promising industrial application value. To highlight the advantage of the ammonia-evaporation method, a Cu/SiO₂ nanocatalyst had been synthesized by a traditional impregnation method for comparison (denoted as Cu/SiO₂-TI; see the preparation process details in the SI). The catalytic activity of Cu/SiO₂-TI nanocatalyst is just 5% at 320 °C, which is much less than that of the Cu/SiO₂-AE nanocatalyst (Figure S4) under the same reaction conditions. Furthermore, the stability of the Cu/SiO₂-

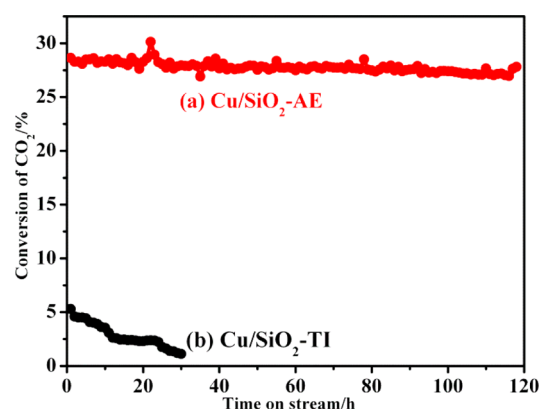


Figure 2. Conversion of CO₂ as a function of time on-stream at 320 °C and 3.0 MPa over the (a) Cu/SiO₂-AE and (b) Cu/SiO₂-TI nanocatalysts.

TI nanocatalyst is quite poor because the catalytic activity is almost completely lost after 25 h (Figure 2). Moreover, the turnover frequency (TOF) values (details shown in the SI) of the Cu/SiO₂-AE and Cu/SiO₂-TI nanocatalysts are 79.85 and 10.44 h⁻¹, respectively. The intrinsic TOF value of the Cu/SiO₂-AE nanocatalyst is 7.7 times as much as that of Cu/SiO₂-TI nanocatalyst, indicating that the Cu/SiO₂-AE nanocatalyst is a high-performance catalyst for CO₂ hydrogenation.

The powder X-ray diffraction (PXRD) patterns of calcined Cu/SiO₂-AE samples reveal that the main peaks centered at $2\theta = 30.8, 35.0, 57.5, \text{ and } 62.3^\circ$ (JCPDS no. 027-0188, Figure 3a),

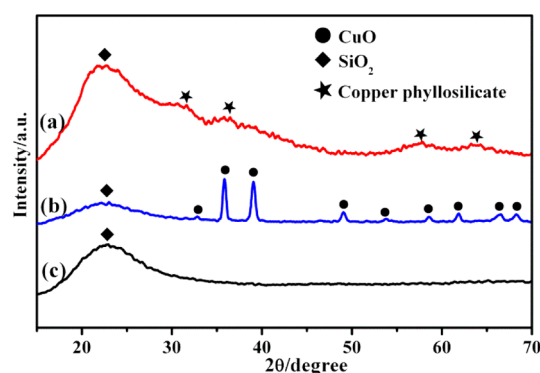


Figure 3. XRD patterns of the (a) calcined Cu/SiO₂-AE sample, (b) calcined Cu/SiO₂-TI sample, and (c) mSiO₂·nH₂O.

which can be indexed to the phase of copper phyllosilicate.²⁹ Meanwhile, there is the phase of CuO ($2\theta = 32.2, 35.2, 38.4, 48.4, 53.2, 58.0, 61.2, 65.9, 67.7^\circ$) (JCPDS no. 044-0706, Figure 3b) in the calcined Cu/SiO₂-TI sample.²⁶ The broad peaks at 22° belong to the amorphous SiO₂ support (Figure 3).²⁶ Fourier-transform IR (FT-IR) spectra were further measured to discriminate Cu species. There are two shoulder peaks at 1040 and 670 cm⁻¹ in the calcined Cu/SiO₂-AE sample (Figure S51a), confirming the existence of copper phyllosilicate.³⁸ There were no corresponding shoulder peaks in the FT-IR spectroscopy of the calcined Cu/SiO₂-TI sample (Figure S51b), suggesting that there was no copper phyllosilicate in the Cu/SiO₂-TI sample.³⁸ Cu 2p X-ray photoelectron spectra (XPS) spectra are shown in Figure 4. The Cu 2p_{3/2} peak binding energy of calcined Cu/SiO₂-AE sample is 935.96 eV (Figure 4a), which is consistent with 936.0 eV of copper phyllosilicate. Meanwhile, the Cu 2p_{3/2} peak binding energy of the calcined

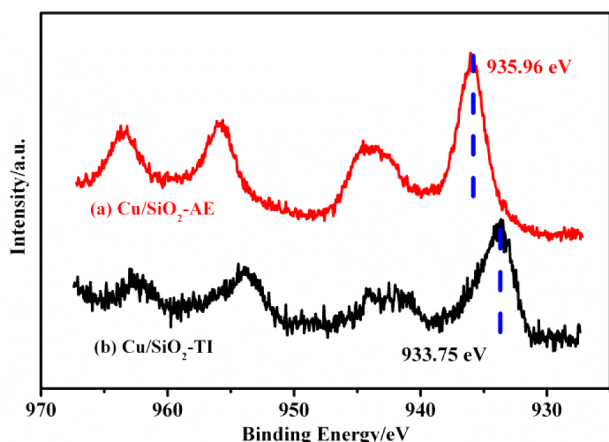


Figure 4. Cu 2p XPS spectra of the calcined (a) Cu/SiO₂-AE and (b) Cu/SiO₂-TI samples.

Cu/SiO₂-TI sample is 933.75 eV (Figure 4b), corresponding to the 933.6 eV of CuO.³⁸

On the basis of the discussion above, we conclude that the main Cu species in the calcined Cu/SiO₂-AE and Cu/SiO₂-TI samples are copper phyllosilicate and CuO, respectively. The Cu 2p_{3/2} peak binding energy shifts from 933.75 to 935.96 eV (Figure 4), demonstrating the existence of interaction between the metal and support in the calcined Cu/SiO₂-AE sample as a result of the formation of copper phyllosilicate (Figures S6, S7).³⁹ The interaction was further proved by the combination of Si 2p XPS (Figure S8), H₂-TPR (Figure S9), PXRD (Figure S10), H₂-TGA (Figure S11), and UV–Vis–NIR diffuse reflectance spectroscopy (Figure S12) characterizations. The existence of interaction can effectively restrain the sintering, which mainly accounts for the long life of the Cu/SiO₂-AE nanocatalyst without any structure promoters.

The FT-IR in Figure S5IIa confirms the disappearance of copper phyllosilicate in the freshly reduced Cu/SiO₂-AE. The PXRD pattern of the freshly reduced Cu/SiO₂-TI nanocatalyst (Figure S13c) shows obvious diffraction peaks at 43.30, 50.44, and 74.10°, which are assigned to Cu (111), (200), and (220) planes (JCPDS no. 070-3039), respectively. The average size of Cu NPs for the Cu/SiO₂-TI nanocatalyst is ~46.5 nm, which is calculated by the Scherrer equation; however, it is worth noting that there are no obvious diffraction peaks for the freshly reduced Cu/SiO₂-AE nanocatalyst except for the diffraction peak at 22° for the SiO₂ support³⁹ (Figure S13a), suggesting that the Cu species are highly dispersed on the surface of the SiO₂. In addition, there are still no obvious diffraction peaks for the Cu/SiO₂-AE nanocatalyst after 120 h of evaluation (Figure S13b).

The transmission electron microscopy (TEM) image of the calcined Cu/SiO₂-AE sample (Figure 5a) exhibits that the copper phyllosilicate presents a lamellar structure, which was formed during the unique ammonia-evaporation process.³⁹ Figure 5b shows the TEM image of the freshly reduced Cu/SiO₂-AE nanocatalyst. The active Cu NPs are homogeneously dispersed on the surface of the SiO₂, with the average size of the Cu NPs being about 2.1 nm, which is ultrasmall among the reported Cu-based nanocatalysts. The active Cu NPs are still highly dispersed on the surface of the SiO₂ after 120 h of evaluation (Figure S14), implying the as-synthesized Cu/SiO₂-AE nanocatalyst is quite stable. On the other hand, the Cu NPs

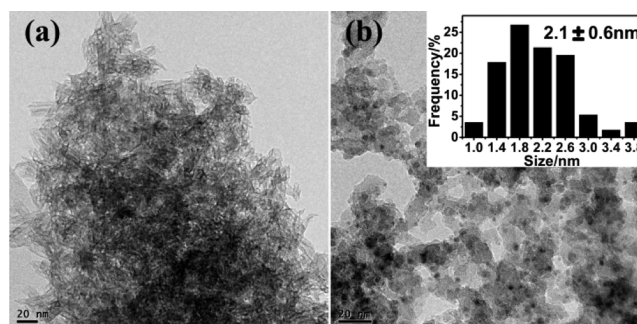


Figure 5. TEM images of the (a) calcined Cu/SiO₂-AE sample and (b) freshly reduced Cu-SiO₂-AE nanocatalyst. The inset shows the corresponding size distribution diagram.

of the freshly reduced Cu/SiO₂-TI nanocatalyst aggregated, and the average size is very large (about 49.5 nm) (Figure S15).

The Cu 2p_{3/2} and Cu 2p_{1/2} peaks of freshly reduced Cu/SiO₂-AE and Cu/SiO₂-TI nanocatalysts appear at 932.8 and 952.7 eV, respectively (Figure S16a), which suggests that the Cu²⁺ species in both calcined Cu/SiO₂-AE and Cu/SiO₂-TI samples can be reduced to Cu⁺ or Cu⁰ species.⁴⁰ The Cu LMM X-ray auger electron spectroscopy (XAES) spectrum is measured to distinguish Cu⁺ and Cu⁰ species.^{41,42} Interestingly, the kinetic energy of Cu/SiO₂-AE nanocatalyst is 914.9 eV, indicating the Cu species is Cu⁺, whereas that of Cu/SiO₂-TI nanocatalyst is 917.6 eV, suggesting the Cu species is Cu⁰ (Figure S16b).^{43,44} In Figure S17, the dominating Cu species after 120 h of time-on-stream is still Cu⁺.

The BET surface area (Table S2; Figures S18, S19) of Cu/SiO₂-AE nanocatalyst is 400.7 m²/g, which is higher than that (335.4 m²/g) of the Cu/SiO₂-TI nanocatalyst, suggesting that the AE method is superior to the TI method for acquiring a higher BET surface area. Interestingly, there are smaller pores (~2 nm) distributed in the Cu/SiO₂-AE nanocatalyst (Figure S20a), and there are no pores of this kind in the Cu/SiO₂-TI nanocatalyst (Figure S20b). The larger BET surface area and small pore size may be a benefit for the CO₂ hydrogenation. Moreover, the Cu dispersion (*D*_{Cu}) and Cu specific surface area (*S*_{Cu}) of Cu⁰ in the Cu/SiO₂-TI nanocatalyst were measured by N₂O titration, whereas those of Cu⁺ in the Cu/SiO₂-AE nanocatalyst were measured by irreversible CO adsorption (Table 1 and Figure S21; see more details in the SI). The *D*_{Cu}

Table 1. Physicochemical Properties of As-Synthesized Nanocatalysts

nanocatalysts	Cu loading (%)	<i>S</i> _{BET} ^a (m ² g ⁻¹)	<i>D</i> _{Cu} ^b (%)	<i>S</i> _{Cu} ^c (m ² g ⁻¹)
Cu/SiO ₂ -AE	10.7	400.7	5.3	31.8
Cu/SiO ₂ -TI	10.1	335.4	3.1	20.8

^a*S*_{BET}: BET surface area of catalysts. ^b*D*_{Cu}: Cu dispersion of catalysts. ^c*S*_{Cu} specific surface area.

of the Cu/SiO₂-AE nanocatalyst is 5.3%, which is higher than the 3.1% of the Cu/SiO₂-TI nanocatalyst (Table 1), and the *S*_{Cu} of the Cu/SiO₂-AE nanocatalyst is 31.8 m²/g, which is also bigger than that (20.8 m²/g) of the Cu/SiO₂-TI nanocatalyst. High-angle annular dark-field scanning transmission electron microscopy (HAADF-STEM) and scanning transmission electron microscopy–energy dispersive X-ray (STEM–EDX) were used to determine the surface distribution of Cu⁺ species in the Cu/SiO₂-AE nanocatalyst (Figures S22, S23). The

relatively high D_{Cu} and S_{Cu} could contribute to the high performance of Cu/SiO₂-AE nanocatalyst.

Three Cu/SiO₂-AE nanocatalysts (Figure S24; see the preparation process in the SI) with different Cu⁺/(Cu⁰ + Cu⁺) ratios have been synthesized to investigate the influence of the valence state. The Cu⁺/(Cu⁰ + Cu⁺) ratio was determined by Cu LMM XAES spectra (Figures S25, S26). Notably, the conversion of CO₂ rapidly increases with an increase in the Cu⁺/(Cu⁰ + Cu⁺) value and reaches the maximum when Cu⁺/(Cu⁰ + Cu⁺) is 1.00, which demonstrates that the Cu⁺ species is the active component in the Cu/SiO₂-AE nanocatalyst for activation and conversion of CO₂ (Figure 6). Considering the reaction was carried out under a reducing

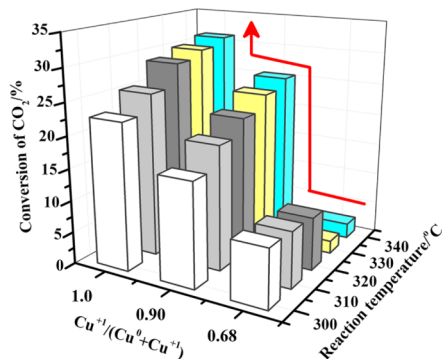


Figure 6. Three-dimensional histogram of conversion of CO₂, Cu⁺/(Cu⁰ + Cu⁺) and reaction temperature.

atmosphere, we changed the reaction temperature of CO₂ hydrogenation to 200 °C and kept the other conditions unchanged. The reaction temperature of 200 °C is lower than the reduction temperature (248 °C) obtained from the H₂-TPR profile (Figure S9). It is worth mentioning that the conversion of CO₂ increased significantly with an increase in the Cu⁺ ratio (Figure S27), which is consistent with the result derived from Figure 6. Therefore, the high ratio of Cu⁺/(Cu⁰ + Cu⁺) is mainly responsible for the high performance of Cu/SiO₂-AE nanocatalyst for CO₂ activation.

In summary, we have successfully synthesized a high-performance and long-lived Cu/SiO₂-AE nanocatalyst for CO₂ hydrogenation by an ammonia-evaporation method without introducing any structure promoters. The Cu⁺ species has been demonstrated to be the active component for the activation and conversion of CO₂. The high value of Cu⁺/(Cu⁰ + Cu⁺) is mainly responsible for the high performance of the Cu/SiO₂-AE nanocatalyst in CO₂ activation. The ultrasmall size, relatively high dispersion, and specific surface area of Cu⁺ species contribute to the high catalytic activity. The interaction between the metal and support mainly accounts for the excellent thermal stability. This work will provide an effective way to synthesize transition-metal-based nanocatalysts (such as Fe, Co, Ni, etc.) with high activity and stability.

■ ASSOCIATED CONTENT

Supporting Information

The Supporting Information is available free of charge on the ACS Publications website at DOI: 10.1021/acscatal.5b00682.

Reaction of CO₂ hydrogenation to methanol; experimental details; BET surface areas; N₂O titration; irreversible CO adsorption measurement; PXRD patterns; TEM images; HAADF-STEM image; STEM-EDX,

XPS, and XAES spectra; H₂-TPR profiles; H₂-TGA profile; UV-Vis-NIR diffuse reflectance spectra (PDF)

■ AUTHOR INFORMATION

Corresponding Authors

*E-mail: znxu@fjirm.ac.cn.

*E-mail: gcguo@fjirm.ac.cn.

Notes

The authors declare no competing financial interest

■ ACKNOWLEDGMENTS

We gratefully acknowledge financial support from the 973 Program (2011CBA00505, 2013CB933200), the NSF of China (21403237, 21303202, 21303203), the NSF of Fujian Province (2014J05025), and Open Project of State Key Laboratory of Supramolecular Structure and Materials (sklssm201506).

■ REFERENCES

- (1) He, M.; Sun, Y.; Han, B. *Angew. Chem., Int. Ed.* **2013**, *52*, 9620–9633.
- (2) Al-mulali, U.; Fereidouni, H. G.; Lee, J. Y. M.; Sab, C. N. B. C. *Renewable Sustainable Energy Rev.* **2013**, *23*, 107–112.
- (3) Dorner, R. W.; Hardy, D. R.; Williams, F. W.; Willauer, H. D. *Energy Environ. Sci.* **2010**, *3*, 884–890.
- (4) Doney, S. C.; Fabry, V. J.; Feely, R. A.; Kleypas, J. A. *Annu. Rev. Mar. Sci.* **2009**, *1*, 169–192.
- (5) Liu, J.; Li, C.; Wang, F.; He, S.; Chen, H.; Zhao, Y.; Wei, M.; Evans, D. G.; Duan, X. *Catal. Sci. Technol.* **2013**, *3*, 2627–2633.
- (6) Falkowski, P.; Scholes, R. J.; Boyle, E.; Canfield, D.; Elser, J.; Gruber, N.; Hibbard, K. *Science* **2000**, *290*, 291–296.
- (7) Omae, I. *Coord. Chem. Rev.* **2012**, *256*, 1384–1405.
- (8) Razali, N. A. M.; Lee, K. T.; Bhatia, S.; Mohamed, A. R. *Renewable Sustainable Energy Rev.* **2012**, *16*, 4951–4964.
- (9) Wang, W.; Wang, S. P.; Ma, X. B.; Gong, J. L. *Chem. Soc. Rev.* **2011**, *40*, 3703–3727.
- (10) Preti, D.; Resta, C.; Squarciarupi, S.; Fachinetti, G. *Angew. Chem., Int. Ed.* **2011**, *50*, 12551–12554.
- (11) Centi, G.; Quadrelli, E. A.; Perathoner, S. *Energy Environ. Sci.* **2013**, *6*, 1711–1731.
- (12) Karelovic, A.; Ruiz, P. *ACS Catal.* **2013**, *3*, 2799–2812.
- (13) He, S.; Li, C.; Chen, H.; Su, D.; Zhang, B.; Cao, X.; Wang, B.; Wei, M.; Evans, D. G.; Duan, X. *Chem. Mater.* **2013**, *25*, 1040–1046.
- (14) Aresta, M.; Dibenedetto, A. *Dalton Trans.* **2007**, 2975–2992.
- (15) Baiker, A. *Appl. Organomet.* **2000**, *14*, 751–762.
- (16) Sakakura, T.; Choi, J. C.; Yasuda, H. *Chem. Rev.* **2007**, *107*, 2365–2387.
- (17) Appel, A. M.; Bercaw, J. E.; Bocarsly, A. B.; Dobbek, H.; DuBois, D. L.; Dupuis, M.; Ferry, J. G.; Fujita, E.; Hille, R.; Kenis, P. J.; Kerfeld, C. A.; Morris, R. H.; Peden, C. H.; Portis, A. R.; Ragsdale, S. W.; Rauchfuss, T. B.; Reek, J. N.; Seefeldt, L. C.; Thauer, R. K.; Waldrop, G. L. *Chem. Rev.* **2013**, *113*, 6621–6658.
- (18) Kleij, A. W. *Catal. Sci. Technol.* **2014**, *4*, 1481–1481.
- (19) Meunier, F. C. *Angew. Chem., Int. Ed.* **2011**, *50*, 4053–4054.
- (20) Gao, P.; Li, F.; Xiao, F.; Zhao, N.; Sun, N.; Wei, W.; Zhong, L.; Sun, Y. *Catal. Sci. Technol.* **2012**, *2*, 1447–1454.
- (21) Arena, F.; Mezzatesta, G.; Zafarana, G.; Trunfio, G.; Frusteri, F.; Spadaro, L. J. *Catal.* **2013**, *300*, 141–151.
- (22) Bansode, A.; Urakawa, A. *J. Catal.* **2014**, *309*, 66–70.
- (23) Gao, P.; Li, F.; Zhan, H.; Zhao, N.; Xiao, F.; Wei, W.; Zhong, L.; Wang, H.; Sun, Y. *J. Catal.* **2013**, *298*, 51–60.
- (24) Liao, F. L.; Huang, Y. Q.; Ge, J. W.; Zheng, W. R.; Tedsree, K.; Collier, P.; Hong, X. L.; Tsang, S. C. *Angew. Chem., Int. Ed.* **2011**, *50*, 2162–2165.
- (25) Grabow, L. C.; Mavrikakis, M. *ACS Catal.* **2011**, *1*, 365–384.
- (26) Baltes, C.; Vukojevic, S.; Schuth, F. *J. Catal.* **2008**, *258*, 334–344.

- (27) Graciani, J.; Mudiyansele, K.; Xu, F.; Baber, A. E.; Rodriguez, J. A. *Science* **2014**, *345*, 546–550.
- (28) Reske, R.; Mistry, H.; Behafarid, F.; Roldan Cuenya, B.; Strasser, P. *J. Am. Chem. Soc.* **2014**, *136*, 6978–6986.
- (29) Yue, H.; Zhao, Y.; Zhao, S.; Wang, B.; Ma, X.; Gong, J. *Nat. Commun.* **2013**, *4*, 2339–2346.
- (30) Chen, C. S.; Lin, J. H.; You, J. H.; Chen, C. R. *J. Am. Chem. Soc.* **2006**, *128*, 15950–15951.
- (31) Zhan, H.; Li, F.; Gao, P.; Zhao, N.; Xiao, F.; Wei, W.; Zhong, L.; Sun, Y. *J. Power Sources* **2014**, *251*, 113–121.
- (32) Behrens, M.; Studt, F.; Kasatkin, I.; Kühn, S.; Hävecker, M.; Abild-Pedersen, F.; Zander, S.; Girgsdies, F.; Kurr, P.; Kniep, B. L.; Tovar, M.; Fischer, R. W.; Nørskov, J. K.; Schlögl, R. *Science* **2012**, *336*, 893–897.
- (33) Behrens, M.; Zander, S.; Kurr, P.; Jacobsen, N.; Senker, J.; Koch, G.; Ressler, T.; Fischer, R. W.; Schlögl, R. *J. Am. Chem. Soc.* **2013**, *135*, 6061–6068.
- (34) Chen, C. S.; Cheng, W. H.; Lin, S. S. *Chem. Commun.* **2001**, *18*, 1770–1771.
- (35) Robbins, J. L.; Iglesia, E.; Kelkar, C. P.; DeRites, B. *Catal. Lett.* **1991**, *10*, 1–10.
- (36) Lin, J. D.; Zhao, X. Q.; Cui, Y. H.; Zhang, H. B.; Liao, D. W. *Chem. Commun.* **2012**, *48*, 1177–1179.
- (37) Behrens, M.; Schlögl, R. *Z. Anorg. Allg. Chem.* **2013**, *639*, 2683–2695.
- (38) Gong, J.; Yue, H.; Zhao, Y.; Zhao, S.; Zhao, L.; Lv, J.; Wang, S.; Ma, X. *J. Am. Chem. Soc.* **2012**, *134*, 13922–13925.
- (39) Zheng, X.; Lin, H.; Zheng, J.; Duan, X.; Yuan, Y. *ACS Catal.* **2013**, *3*, 2738–2749.
- (40) Chen, L. F.; Guo, P. J.; Qiao, M. H.; Yan, S. R.; Li, H. X.; Shen, W.; Xu, L. H.; Fan, K. N. *J. Catal.* **2008**, *257*, 172–180.
- (41) Yue, H.; Ma, X.; Gong, J. *Acc. Chem. Res.* **2014**, *47*, 1483–1492.
- (42) Yin, A. Y.; Guo, X. Y.; Fan, K. N.; Dai, W. L. *ChemCatChem* **2010**, *2*, 206–213.
- (43) Huang, Y.; Ariga, H.; Zheng, X.; Duan, X.; Takakusagi, S.; Asakura, K.; Yuan, Y. *J. Catal.* **2013**, *307*, 74–83.
- (44) Yin, A. Y.; Guo, X. Y.; Dai, W. L.; Fan, K. N. *J. Phys. Chem. C* **2009**, *113*, 11003–11013.